Florice Nzikou Mouketou¹ / Andrei Kolesnikov¹

Modelling and Simulation of Multiphase Flow Applicable to Processes in Oil and Gas Industry

¹ Department of Chemical, Metallurgical and Materials Engineering, Faculty of Engineering and the Built Environment, Tshwane University of Technology, Pretoria, South Africa, E-mail: floricenm@gmail.com, kolesnikova@tut.ac.za

Abstract:

Solid particle erosion is a mechanical process of destroying a wall surface material due to the impacts of solid particles entrained with a fluid. It is a frequent phenomenon encountered within various industries such as chemical processes, oil and gas, and hydraulic transportation. Erosion problem has led to enormous consequences such as oil spills caused by equipment failure of oil transmission pipelines, chokes valves, pipe fittings etc; resulting in considerable economic loss as well as safety and environmental concerns. In this study, a 3-D simulations are performed using CFD code ANSYS FLUENT to predict sand erosion rates under different engine-oil viscosity conditions for multiphase liquid, in a 90-degree standard (R/D = 1.5) elbow pipe. The CFD utilizes Eulerian-Lagrangian method to model the multiphase flow oil-water-sand in elbow. The realizable k- ϵ model is adopted for the fluid turbulence effects. The velocity and pressure distributions are analysed as contours for the fluid flow. In order to understand the dynamics of the erosion process, the motion of the solid particles are also investigated based on Stokes number as well as the effect of secondary flows. The results indicated that erosion rates decrease with the increase in oil viscosity. Additionally, erosion mainly occurs in two locations; at the extrados near the bend exit and also on the side walls of the downstream straight pipe. The unusual distribution of erosion on the side walls occurred as a result of the effect of secondary flows due to centrifugal force. The numerical results are in qualitative good agreement with the experimental data available in the literature for elbows in order to validate the presented modelling approach.

Keywords: solid particle erosion, oil viscosity, multiphase flow, CFD, elbow

DOI: 10.1515/cppm-2017-0066

Received: September 26, 2017; Revised: June 15, 2018; Accepted: August 11, 2018

1 Introduction

The presence of solid particle often occurs in most industrial processes involving fluid flows. Typically in the petroleum industry, sand particle is frequently produced and entrained along with crude oil and natural gas through pipelines transportation before reaching any process equipment. During the multiphase flow (presence of more than one phase), particles obtain momentum from the carrier fluid and flow along to impinge on the inner wall of the pipes, fittings, valves, and other pumping devices by causing wear to these facilities. In fact, erosion is a wear damage caused by moving particles which strike the inner surface of a material [1]. Especially pipe bends such as elbows are the most vulnerable to solid erosion damage due to the significant effect of pressure drop, centrifugal effects, and the sudden alter of direction in flow field [1, 2]. Consequently, erosion damage has been a major problem in the oil and gas industry due to equipment failure which may lead to potential oil spillage, operating problems, production loss, resulting in great financial losses as well as safety and environmental concerns [3]. Therefore, it is crucial to comprehend the nature and severity of erosion in pipe elbows to predict accurately the erosion rates and identify the locations the most affected around the bend, in order to further evaluate the lifespan of this facility [4].

Solid particle erosion is a complex mechanical process in which the severity of the damage may depend on a wide range of parameters, such as the operating conditions, fluid properties, solid particle properties, multiphase flow regime, wall target material, and its geometry [5]. The erosion process can be investigated experimentally via laboratory tests, or numerically using computer based simulations, as well as using mathematical empirical equations, given that the flow parameters are contained in the model [6]. Blanchard *et al.* [7] conducted an experimental analysis of erosion process of a 90-degree pipe bend by solid particles entrained in water. The experimental results indicated that the erosion for a pipe elbows whose R/D ratio is 1.5, the maximum wear point is located at an angle of 85-degree in average on the bend.

Furthermore, since experimental work is costly and cannot be represented in an industrial scale, many researchers have conducted significant numerical studies using Computational Fluid Dynamics (CFD) to predict erosion caused by solid particles in multiphase gas or liquid flow in pipe bend. In gas flow, Solnordal et al. [8] carried out a detail experimental and numerical analysis of erosion caused by sand using air as the conveying fluid in a standard pipe elbow. It was found that the erosion depth and distribution of the numerical modelling agreed well with the experimental data only when a suitable rough wall collision model was adopted, or else it lead to inaccurate prediction. The erosion model used in their work is the well known model expressed by Finnie that has been widely used to predict erosion rate for pipe bend. Parsi et al. [9] applied a CFD-based sand particle erosion for elbow in gas-dominant multiphase flow of low, medium, and high gas flow rates using six different erosion equations to find out which equation provides the best prediction. It was observed that the Mansouri et al. [10] erosion equation provided the best predictions when compared with the experimental data. The Grant and Tabakoff [11] remarkably over predicted the maximum erosion rate, and the remaining models Neilson and Gilchrist [12], Oka et al. [13], DNV [14], and Zhang et al. [15] under predicted the maximum erosion rates. In liquid flow, Peng and Cao [16] applied a CFD-based numerical simulation of solid particle erosion in pipe bends for liquid-solid flow system. They used five different erosion models to predict the erosion rate, and it was found out that the erosion model with the Grant and Tabakoff particle-wall rebounded model produced closer results to the experimental data. Wang et al. [2], investigated numerically the erosion behaviour in elbows of petroleum pipelines using CFD to assess the effects of bend orientation and particle properties on the erosion process. They found out that the maximum erosion rate is located near the elbow exit. Similar results were also found by Chen et al. [1], when they used CFD-DEM coupling method. In addition, Peng Jr et al. [5], performed a CFD analysis of erosion in multiphase flow and compare their promising agreement obtained between numerical results of erosion rate and the empirical predictions. They also indicated that the empirical models, API RP 14E, Salama, and DNV RP-0501 are more applicable in high liquid flow (liquid volume > 5%total volume).

However, most current studies on CFD-based erosion models and experimental data available in the literature focus more on gas-dominant operating conditions and on single phase, gas or water liquid phase as the carrying medium than in multiphase liquid situations [5]. More investigations may need to be carried out on solid particle erosion in multiphase liquid situations in this field. In particular, the study of sand erosion in oil-water flow has rarely been reported in the literature. Furthermore, only few studies have conducted a comprehensive analysis on the effect of liquid viscosity on elbow erosion. Therefore, this numerical work attempts to cover the area in which oil phase is taken into consideration, which has drawn little attention in the field. The study presents a CFD-based erosion modelling approach due to the presence of sand particles entrained in multi-component liquid phase oil-water. The aim of the study is to predict sand erosion rates in a 90-degree elbow pipe and the maximum erosion location for different engine-oil viscosity conditions. A three-dimensional simulation is performed using finite volume method with realizable k-ɛ turbulence model with Eulerian-Lagrangian modelling approach. Due to the lack of experimental data in the literature, a simulation case involving only solid particle and water in elbow is carried out and compared with the experimental data of Blanchard *et al.* [7] for verification purpose.

2 Computational modelling

In general, CFD-based sand erosion under multiphase flow consists of three major steps: the fluid flow modelling, the particle motion modelling and the erosion modelling. According to Mohyaldin *et al.* [6], CFD simulation of sand erosion is usually achieved in four steps. In the first step, the model is built and divided into sub domain using a grid generation. The second step involves the fluid flow modelling (oil-water) treated as a continuous phase and solved by the Reynolds average Navier-Stokes (RANS) equations in Eulerian framework, while the third step involves the particle tracking, treated as a discrete phase and captured by the discrete phase model (DPM) in a Lagrangian framework. And finally, the last step involves the erosion calculation that relates the particle impact information such as the angle and velocity of impingement introduced to a selected erosion prediction model. The CFD simulations are carried out using the commercial software package ANSYS Fluent 17.2.

In addition, some modelling assumptions involving the CFD simulations are stated as follow:

- The simulation is performed under steady state conditions.
- No effect of temperature change on the flow has been considered and isothermal conditions have been assumed.

Automatically generated rough PDF by ProofCheck from River Valley Technologies Ltd

- The particles do not affect the fluid flow, thus a one-way coupling is applied for all the simulations. The flow is much diluted, the volume fraction of the sand particles and particle-particle interaction are negligible.
- The fluid (water-oil) is considered as a continuous primary phase, whereas sand particle is the discrete secondary phase, sand particles are assumed to be smooth and spherical in shape and are uniformly distributed in liquid phase.
- The drag and gravity forces are the most important forces acting on the particle.
- There is no-slip boundary condition at the wall of the pipe elbow.

2.1 Computational geometry and mesh generation

A 3-D geometry was created in ANSYS DesignModeler using the same computational geometry dimensions of an elbow pipe used in the study conducted by Wang $et\,al.$ [2]. The model geometry is a 90° standard elbow pipe (R/D = 1.5) with an internal diameter of 40 mm and a curvature radius of 60 mm. In order to achieve a fully developed flow, the lengths of 400 mm (10D) for both horizontal pipe upstream and vertical pipe downstream of the elbow were used. The general flow conditions are shown in Table 1.

Table 1: General flow conditions.

Description	Value
Pipe material	Aluminium (Fluent default)
Pipe diameter, D (mm)	40
Bend radius, R (mm)	60
Length of horizontal straight pipe (mm)	400
Length of vertical straight pipe (mm)	400
Carrier fluid (primary phase)	Water
Fluid density, ρ (kg/m ³)	998.2
Inlet velocity, u _w (m/s)	30
Carrier fluid (secondary phase)	Engine oil
Inlet velocity, u _o (m/s)	30
Particle density, ρ_p (kg/m ³)	2650
Particle diameter, d _p (μm)	150
Particle flow rate, m_p (kg/s)	0.2

¹ Experimental data

The grid was defined to provide a reduced solving time and increase the accuracy of the numerical solution. A finer grid scheme was created near the pipe wall with five (5) inflation-layers to obtain an accurate flow field near the pipe wall and provide a better erosion prediction [16]. The entire computational domain was discretised using hexahedral grid type. Hexahedral mesh has the advantage of providing high-quality solution with less number of computational cells and it is generally more aligned with the flow. The total number of nodes in the model was 108 315, with 306 109 faces and 103 912 cells.

2.2 Flow field modelling

The liquid is treated as a continuous phase and modelled by solving the Navier-Stokes conservation of mass and momentum equations for fully developed incompressible pipe flow. Taking into account the volume fraction of the liquid phases, the conservation equations are expressed as follows [1, 17].

$$\frac{\partial}{\partial t} \left(\alpha_f \rho_f \right) + \nabla \cdot \left(\alpha_f \rho_f \vec{u}_f \right) = 0 \tag{1}$$

$$\frac{\partial}{\partial t} \left(\alpha_f \rho_f \vec{u}_f \right) + \nabla \cdot \left(\alpha_f \rho_f \vec{u}_f \vec{u}_f \right) = -\alpha_f \nabla P + \nabla \cdot \left(\alpha_f \bar{\tau}_f \right) + \alpha_f \rho_f \vec{g}$$
 (2)

$$\alpha_w + \alpha_o = 1 \tag{3}$$

Where α is the volume fraction, ρ is the density, \vec{u} is the velocity vector, P is the static pressure, $\bar{\tau}$ is the stress tensor, and $\rho \vec{g}$ is the gravitational body force. The subscript f represents the liquid phase: water (W) and oil (O).

The stress tensor $\bar{\tau}$ is calculated as follows:

Where μ is the molecular fluid viscosity, I is the unit tensor, and the second term on the right hand side is the effect of volume dilation.

The realizable k- ϵ two-equation model is adopted to describe the kinetic energy encountered in the continuous phase and dissipated in the dispersed phase. And the standard wall function approach is used to model the flow in near-wall region. The modelled transport equations for k and ϵ in the realizable k- ϵ model are as follows:

Turbulent kinetic energy transport equation:

$$\frac{\partial}{\partial t} \left(\alpha_f \rho_f k \right) + \nabla \cdot \left(\alpha_f \rho_f u_f k \right) = \nabla \cdot \left[\alpha_f \left(\mu + \frac{\mu_t}{\sigma_k} \right) \nabla k \right] + \alpha_f G_k - \alpha_f \rho_f \varepsilon + \alpha_f S_k$$
 (5)

Dissipation of turbulent kinetic energy transport equation:

$$\frac{\partial}{\partial t} \left(\alpha_f \rho_f \varepsilon \right) + + \nabla \cdot \left(\alpha_f \rho_f u_f \varepsilon \right) = \nabla \cdot \left[\alpha_f \left(\mu + \frac{\mu_t}{\sigma_{\varepsilon}} \right) \nabla \varepsilon \right] + \alpha_f \rho_f C_1 S_{\varepsilon} - \alpha_f \rho_f C_2 \frac{\varepsilon^2}{k + \sqrt{v\varepsilon}} + \alpha_f S_{\varepsilon}$$
 (6)

The turbulent eddy viscosity is computed from:

$$\mu_t = \rho C_\mu \frac{k^2}{s} \tag{7}$$

In the above equations, G_k represents the generation of turbulence kinetic energy due to the mean velocity gradients, C_2 and C_1 are constants, σ_k and σ_{ε} are the turbulent Prandtl numbers for k and ε , S_k and S_{ε} are the user-defined source terms. Turbulence model coefficients are given in the Table 2.

Table 2: Coefficients for realizable k-ε turbulent model.

$C_{1arepsilon}$	C_2	σ_k	$\sigma_{arepsilon}$	C_{μ}
1.44	1.9	1.0	1.2	0.09

2.3 Particle tracking

The motion of the particles in discrete phase is described by the Newton's laws of motion which is the sum of all fluid-solid interaction forces. For the purpose of this study, the motion of a particle in fluid is mostly affected by the drag force. The governing equation of particle motion proposed by Newton's second law is:

$$\frac{d\vec{u}_p}{dt} = F_D \left(\vec{u}_f - \vec{u}_p \right) + \overrightarrow{F_g} + \overrightarrow{F_P} + \overrightarrow{F_{VM}}$$
(8)

In the expression, the first term on the right hand side represents the drag force, $\overrightarrow{F_D}$, caused by the velocity difference of the fluid and the particles, and the other terms $\overrightarrow{F_g}$, $\overrightarrow{F_P}$ and $\overrightarrow{F_{VM}}$ represent the gravity force, the pressure gradient force and the Virtual mass force, respectively.

The drag force is the most dominant term computed by the following relationship:

$$\overrightarrow{F_D} = \frac{18\mu}{\rho_v d_v^2} \frac{C_D R e_p}{24} \left(\overrightarrow{u}_f - \overrightarrow{u}_p \right) \tag{9}$$

The drag coefficient, C_D , in this study is expressed based on spherical drag law for smooth sand particles as the following equation:

$$C_D = a_1 + \frac{a_2}{Re} + \frac{a_3}{Re^2} \tag{10}$$

Where a_1 , a_2 and a_3 are constants that are applied over a wide range of Re given by Morsi and Alexander [18]. Re is the particle Reynolds number calculated from the following relationship:

$$Re = \frac{\rho_f d_p \left| \vec{u}_f - \vec{u}_p \right|}{u} \tag{11}$$

Where u_p is the particle velocity, d_p is the particle diameter, ρ_p is the density of the particles, ρ_f and μ are the density and viscosity of the fluid, respectively.

The gravity force is expressed as:

$$\overrightarrow{F_g} = \frac{\left(\rho_P - \rho_f\right)}{\rho_p} \vec{g} \tag{12}$$

Which is computed by the difference in sand particle density (ρ_P) and the density of the fluid (ρ_f) The pressure gradient is defined as:

$$\overrightarrow{F_P} = \left(\frac{\rho_f}{\rho_v}\right) \nabla P \tag{13}$$

The virtual mass force can be expressed as:

$$\overrightarrow{F_{VM}} = \frac{1}{2} \frac{\rho_f}{\rho_p} \frac{d\left(\vec{u}_f - \vec{u}_p\right)}{dt} \tag{14}$$

2.4 Particle-wall collision and erosion model

During particle-wall collision, particles hit the wall surface of the material and then rebound back to the fluid domain. Due to the effects of the impact, particles lose some kinetic energy; the rebound velocity is always lower than the incident velocity. This impact is characterized by the change in particle momentum through the coefficients of restitution, e_n and e_t for the normal and tangential velocity components, respectively [16, 19]. e_n and e_t are written as:

$$e_n = \frac{u_{pn2}}{u_{pn1}} \tag{15}$$

$$e_t = \frac{u_{pt2}}{u_{pt1}} \tag{16}$$

Where u_{pn} and u_{pt} are the normal and tangential velocity components of the particle, respectively. Subscript 1 refers to the condition prior collision and subscript 2 is after collision.

In this study, the restitution coefficients in the normal and tangential directions to the wall are the default correlations by Ansys Fluent, as follows:

$$e_n = 0.993 - 0.0307\alpha + 0.000475\alpha^2 - 0.00000261\alpha^3$$
(17)

$$e_t = 0.988 - 0.029\alpha + 0.000643\alpha^2 - 0.00000356\alpha^3$$
(18)

Where α is the particle impact angle.

When the particles impact the wall material, the impact information such as location, velocity and angle of impingement is recorded in each CFD cell next to the pipe wall. These data are then introduced to the selected erosion equation monitored at the wall boundaries. The erosion equation model used in this study is the default equation provided by Fluent, defined as follows:

$$R_{erosion} = \sum_{p=1}^{N \ Particles} \frac{\dot{m}_p C\left(d_p\right) f\left(\alpha\right) v^{b(v)}}{A_{face}} \tag{19}$$

Where:

- $C(d_p)$: particle mass flow rate

– α : impact angle of particle path with the wall face

- $f(\alpha)$: function of impact angle

v : relative particle velocity

-b(v): function of relative particle velocity

- A_{face} : area of cell face at the wall subject to erosion

C, f and b are the constant functions defined as part of the wall boundary conditions and their numerical values based on the pipe material used. The values of the functions C, f and b are 1.8E-09, 1, and 0, respectively, as specified in Ansys Fluent guide.

A piecewise-linear profile in Fluent is used to define the impact angle function found in the literature, as given in Table 3. The diameter function is defined at the value of 1.8E-9 and the velocity exponent is set at the constant value of 2.6 because it is consistent with the value in the open literature for sand.

Table 3: Point values for impact angle function [20].

Point	Angle	Value
1	0	0
2	20	0.8
3	30	1
4	45	0.5
5	90	0.4

3 Boundary conditions

Four boundary conditions have been selected for the calculation domain. The Inflow boundary is where the fluid flow is solved and the particles are injected and tracked along the flow up to the Outflow boundary. And the wall boundaries (Inner and Outer) are used to account for the erosion simulation. At the inlet boundary oil and water are initially introduced at the same velocity [2], and the particle with a density of $2650 \, \text{kg/m}^3$ are initially released uniformly at the same fluid velocity. Water and oil are used as primary phase with their local volume fractions of $65\,\%$ and $35\,\%$ respectively.

The operating pressure is set as $1.01E + 05\,Pa$ (atmospheric condition) and the pressure outlet boundary condition is set as zero with a gauge pressure at the outlet. A no-slip boundary condition is applied on the wall to model the oil-water flow. Since the flow is fully developed, Intensity and Hydraulic diameter method is used with turbulent intensity set as default value of $5\,\%$ and hydraulic diameter of $0.04\,m$. In addition, the wall roughness height is set as $10\,\mu m$, the roughness constant of $0.5\,$ is a default value, and the wall boundaries are set as "reflect" and the outlet boundary as "escape"[16].

Automatically generated rough PDF by ProofCheck from River Valley Technologies Ltd

4 Simulation procedure and convergence

The numerical solutions are obtained by simulating first the fluid flow (oil-water) and secondly sand particles are injected from the inlet surface of the pipe. Four simulation cases are presented for different engine oil SAE 15W-40 viscosity conditions as shown in Table 4 to predict how the erosion is affected. The phase coupled SIMPLE algorithm is employed to solve the pressure-velocity coupling for multiphase flow. A second order upwind scheme is used for the discretization of the different equations to ensure a better accuracy of the numerical solution [2]. A surface monitor for static pressure is defined at the outlet boundary [21]. Additionally, the Number of Continuous Phase Iterations per DPM Iteration is set to 5 and 10,000 for Maximum Number of Steps in tracking parameters. The simulations are executed in the Intel (R) Xeon (R) with specifications of CPU E5-2697 2.60 GHz and 128 GB RAM with Windows Server 2007 platform.

Table 4: CFD runs at different oil viscosity conditions.

CFD run	Fluid	Viscosity (Pa.s)	Density (kg/m³)	Velocity (m/s)	<i>d_p</i> (μm)	ρ_p (kg/m³)	<i>i</i> n _p (kg/s)
1	Water	0.001003	998.2	30	150	2650	0.2
	Oil@50°C	0.057172	860.2	30			
2	Water	0.001003	998.2	30	150	2650	0.2
	Oil@40°C	0.091057	866.3	30			
3	Water	0.001003	998.2	30	150	2650	0.2
	Oil@30°C	0.155310	872.5	30			
4	Water	0.001003	998.2	30	150	2650	0.2
	Oil@20°C	0.287230	878.7	30			

5 Results and discussion

5.1 Model verification

A verification case is carried out to validate the numerical model presented in this study under the same experimental conditions analysed by Blanchard $et\,al.$ [7]. They conducted this experimental analysis of erosion process of a 90-degree pipe elbow with various sand particle sizes ranging from 95 μ m to 605 μ m in diameter. They found out that the maximum point, at which erosion occurs, is located to be at an average angle of 85-degree, measured from the starting point of the curve. Furthermore, the results indicated that for an elbow whose R/D ratio is 1.5, a consistency was observed in the location point of the maximum wear.

The verification case for erosion prediction involves two phase flow particle-water, simulated using CFD code in a 90-degree pipe elbow with R/D ratio equal to 1.5. The pipe diameter is 25.4 mm, and the curvature radius is 38.1 mm. The fluid with an inlet velocity of 5 m/s, enters from the vertical downstream pipe and discharges horizontally with lengths straight pipe of 10D each (D is the inner diameter of the pipe). The solid particles of $605\,\mu m$ in size with density of $2500\,kg/m^3$, are injected uniformly at the pipe inlet with the same velocity as the fluid and a mass flow rate of $0.1\,kg/s$ [2, 7]. The numerical solution was obtained after 200 iterations.

The comparison of the erosion profile between the predicted numerical results and the experimental data along the wall of the elbow can be seen in Figure 1. It can certainly be shown that there is a similar tendency between the predicted results and the experimental data. In addition, the maximum wear location occurs at the exit of the elbow (pick point of the graphs) at an average angle $\phi = 86^{\circ}$, measured from the starting point of the bend wall. Comparably, the maximum erosion depth occurs at the average angle $\phi = 85^{\circ}$ of the bend wall in the experiment. However, discrepancies can be observed (under prediction) between CFD predictions and actual measured values of erosion depths. This may be due to the dissimilarities in wear coefficient and mostly the velocity exponents between Finnie erosion equation used for the experiment and the erosion equation provided by Fluent used in the CFD modelling at the wall boundary. Additionally, the authors indicated that the 2-D experimental model failed to account for the secondary flow effects which were present, whereas the present study in 3-D successfully predicted these flows. Therefore, these reasons are suspected to be the causes of the lower CFD erosion depths prediction by two orders of magnitude compared with the experimental erosion depths.

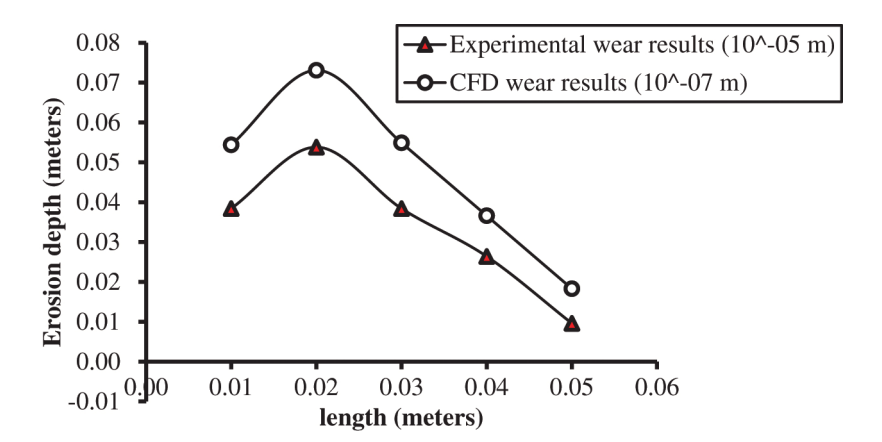


Figure 1: Comparison of erosion depth profile between simulation results with experimental data of Blanchard et al. [7].

5.2 Flow analysis of oil-water in elbow pipe

Figure 2(a-d) below shows the contours of volume fraction of oil and water at different oil viscosity conditions. It can commonly be observed in each case that the horizontal upstream section of the pipe presents a constant green colour for the water volume fraction and a constant yellow colour for oil volume fraction. Since the water volume fraction in that section is about 65%, thus the remaining 35% of the flow is oil when we are looking at the contours. Therefore, oil and water are fully mixed. The mixed flow is developed before and after the bend with insignificant change in volume fraction of each phase. In addition, Figure 3 illustrates the velocity contours of oil and water which indicate that the phases are flowing at the same velocity. However, oil and water are two immiscible fluids due to the difference in physical properties. The flow may be suspected to form emulsions favour by the high velocity, in which tiny oil droplets could be dispersed in water since in this case water occupies 65% of the total volume in the pipe. Therefore, this result comes into agreement with Nädler and Mewes [22], that the flow characteristic of oil and water in pipes highly depends on the volume fraction and droplet distribution of the dispersed phase because of the density difference between the two phase.

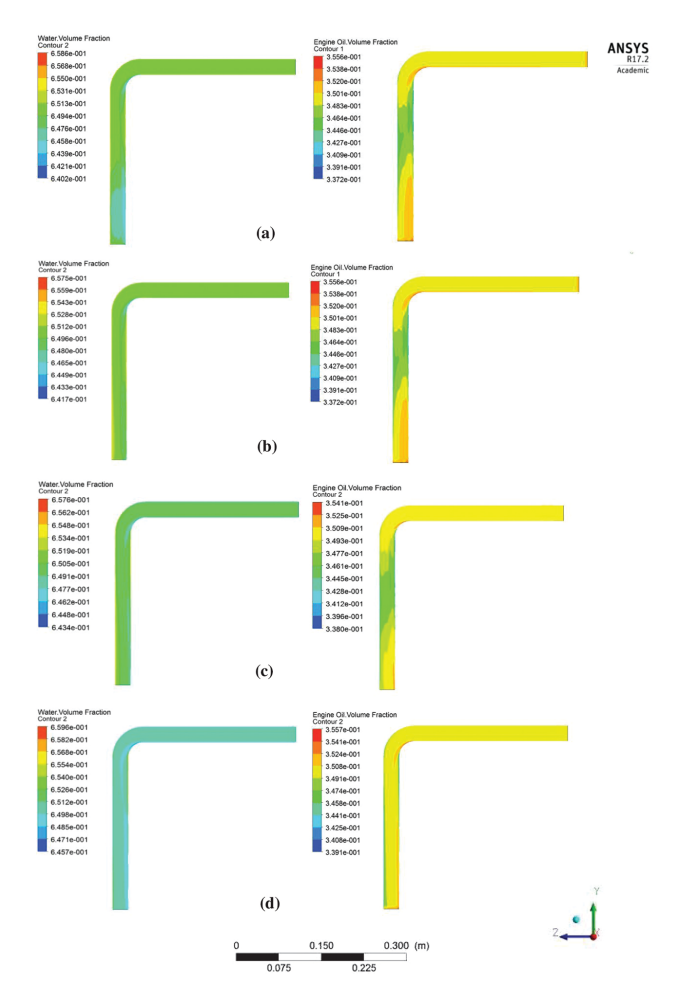


Figure 2: Contours of volume fraction of oil and water at different oil viscosity conditions in symmetric plan: (a) 0.0572 Pa.s, (b) 0.0911 Pa.s, (c) 0.155 Pa.s, (d) 0.287 Pa.s.



Figure 3: Velocity distribution of oil and water in symmetric plan at different oil viscosity conditions: (a) 0.0572 Pa.s, (b) 0.0911 Pa.s, (c) 0.155 Pa.s, and (d) 0.287 Pa.s.

Furthermore, due to the effects of oil viscosity increase in the model, the shear stress (τ) is developed by the friction between the fluids particles and consequently induce pressure drop in pipe. Because of the viscous stress created along the pipe, according to Newton's law of viscosity, the fluid (oil-water) molecules interact and exchange momentum with the discrete phase sand particle by the influence of viscosity and velocity gradient, through the linear relationship in eq. (20). Additionally, high oil viscosity might produce the presence of oil film with the tendency to stick on the pipe wall, thus reduce the kinetic energy of the solid particle to collide on the wall bend [23].

$$\tau\left(y\right) = \mu \frac{du_{x}}{dy} \tag{20}$$

Where, μ is the dynamic viscosity (coefficient of viscosity), u_x is the flow velocity along the boundary, and y is the height above the boundary.

5.3 Velocity distribution along the elbow

The results of velocity distribution for different oil viscosity conditions are shown in Figure 3(a-d) as symmetry plane. The magnitude of the velocity of the continuous phase is clearly indicated by the colour. It can be observed that the maximum velocity zone is developed at the inner wall (intrados) of the bend and a lower velocity zone is developed at the outer wall (extrados), with a separation of a clear boundary layer. The maximum velocities at the intrados are $40.23 \,\text{m/s}$, $40.43 \,\text{m/s}$, $40.76 \,\text{m/s}$ and $41.01 \,\text{m/s}$ for (a), (b), (c) and (c), respectively and tend to slightly increase with the oil viscosity. This numerical profile is in qualitative good agreement with the experimental results by Enayet et~al. [24] for flow behaviour in a pipe bend. The high velocity near the intrados of the bend can be initially explained by the sudden change in flow direction; hence the flow becomes more turbulent in that zone than in the horizontal upstream and vertical downstream zones. In the circular

utomatically generated rough PDF by *ProofCheck* from River Valley Technologies Ltd

cross-section the pressure distribution becomes uneven and the high velocity is directing the flow from intrados to extrados of the pipe due to the action of centrifugal force. Additionally, the presence of secondary flow is expected in that region of the pipe, as a result of high velocity pattern close to the intrados of the bend [25].

5.4 Pressure distribution along the elbow

The static pressure distribution along the pipe domain can be shown in Figure 4(a-d) for different viscosity conditions. The contours show that the maximum pressure at the inlet of the pipe elbow is generally increased with the increase in oil viscosity. The common trend observed in each case is that the pressure drops gradually along the flow direction. At the bend section the direction of the fluid is changed and this in manifested by the migration of the fluid and solid particle from the inner to the outer side of the bend. Thus, the motion of the fluid is under the effect of centrifugal force as a result of inertia. This makes the static pressure on the extrados higher than that near the intrados, as is indicated in Figure 4 [26]. The local static pressures located at the extrados of the bend are 3.95E + 05 Pa, 4.14E + 05 Pa, 5.10E + 06 Pa, and 6.52E + 05 Pa with the respective increase of oil viscosity. In addition, when the fluid exits the bend the static pressure along the vertical downstream straight pipe will not restore its original state due to inertia effect. Therefore, the colour in the contours indicates that the static pressure is gradually decreasing along the flow direction as a result of friction [27].

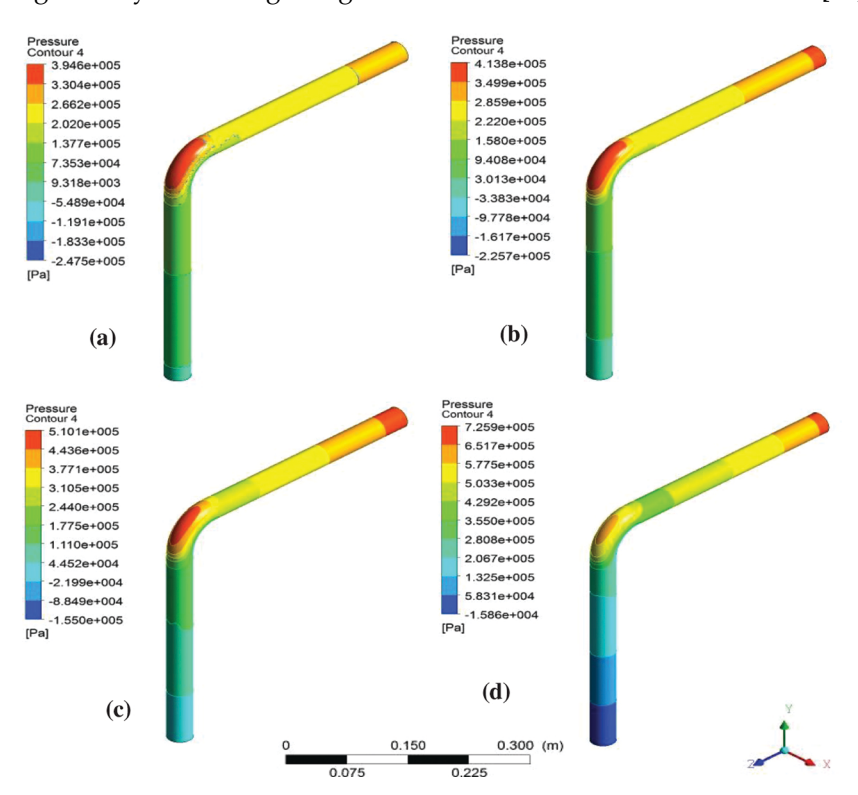


Figure 4: Pressure distribution in the elbow for different oil viscosity conditions: (a) 0.0572 Pa.s, (b) 0.0911 Pa.s, (c) 0.155 Pa.s, and (d) 0.287 Pa.s.

5.5 Effect of oil viscosity on erosion rates

The increase in oil viscosity clearly demonstrates that it has a significant influence on the erosion rates of solid material. It can be shown in Figure 5 below that, erosion rate decreases with the increase in oil viscosity. It is worth noticing that when oil viscosity is increased from 0.0572 Pa.s to 0.09106 Pa.s, the maximum erosion rate on the elbow is slightly decreased from 3.24E-05 kg/m².s to 3.035E-05 kg/m².s and then drastically decreases to 2.154E-05 kg/m².s when the viscosity is increase to 0.155 Pa.s. This result indicates that the viscous fluid reduces the potentiality of the sand particle to strike on the pipe wall, resulting in a decrease of material failure [28]. Furthermore, the motion of the sand particle is given by the surrounding liquid phase through the drag force due to their relative velocity difference. This may imply that, as the fluid becomes more viscous it restricts the motion of the particles and reduces particle kinetic energy, hence their ability to erode [29]. In addition, a presence of liquid film may be expected to form at the wall surface of the elbow with a finer grid generation.

As the carrier liquid mixture becomes viscous, the liquid film also becomes thicker. As a result, the liquid film slows the particle's impact velocity [30].

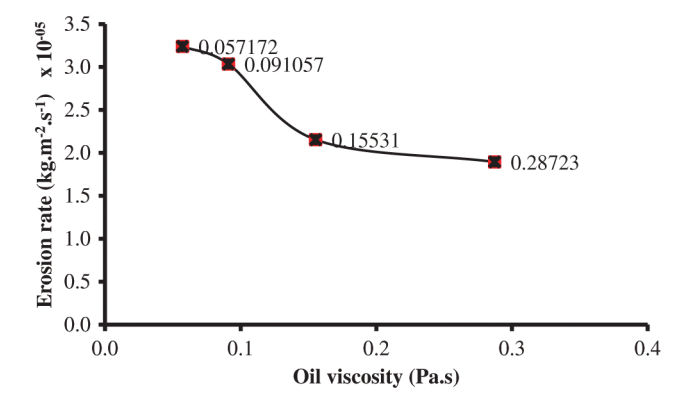


Figure 5: Effect of oil viscosity on erosion rate.

5.6 Distribution of erosion rate and location of maximum wear point

Erosion rate distributions on the walls of the elbow are presented as contours in Figure 6. The contours clearly show that, erosion is distributed on the extrados and on side walls of the downstream straight pipe near the bend exit for all simulations. Erosion is negligible on the upstream and downstream straight pipes, since the solid particles are flowing along the fluid streamlines parallel to the pipe axis, whereas the bend wall is more vulnerable due to the change in flow direction. In addition, the erosion rates per unit area reach their maximum values of $3.24\text{E}-05\,\text{kg/m}^2.\text{s}$, $3.035\text{E}-05\,\text{kg/m}^2.\text{s}$, $2.154\text{E}-05\,\text{kg/m}^2.\text{s}$ and $1.895\text{E}-05\,\text{kg/m}^2.\text{s}$, respectively at the extrados near the bend exit, approximately at an average angle of 87-degree measured from starting point of the bend, as further illustrated in Figure 6. Therefore, the maximum erosive locations occur at an average angle of 87-degree, which is in reasonable agreement with the experimental data of Blanchard *et al.* [7].

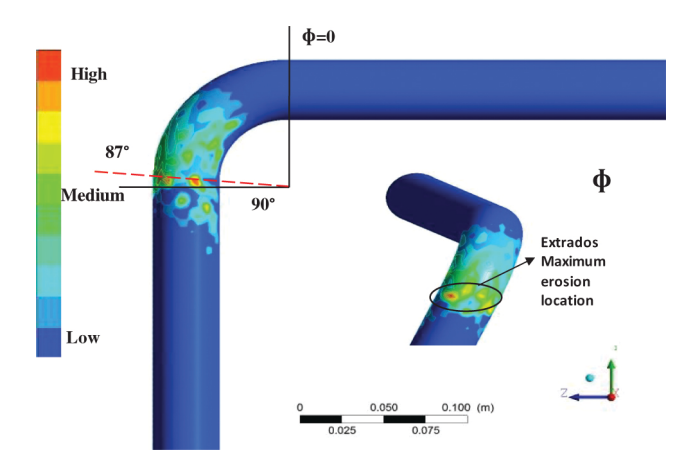


Figure 6: Maximum erosion location on the elbow.

A sample particle trajectory is displayed in Figure 7 in order to analyse the motion of the particle in the flow field for the erosion phenomenon. The trajectories of the particles are mostly governed by the continuous phase through the drag force. When approaching the bend, the flow is fully developed, and the solid particles have sufficient momentum and also the sudden change in flow direction causes them to deviate from the fluid streamlines. Therefore, the solid particles impinge directly on the extrados near the bend exit and cause severe erosion in location A as illustrated in Figure 7. Moreover, the secondary flows due to centrifugal effects inside the bend section drive a number of particles in a circular motion. Hence, the effects of secondary flow convey the particles to the side walls of the downstream straight pipe near the exit and as a result, causing erosion in location B [2].

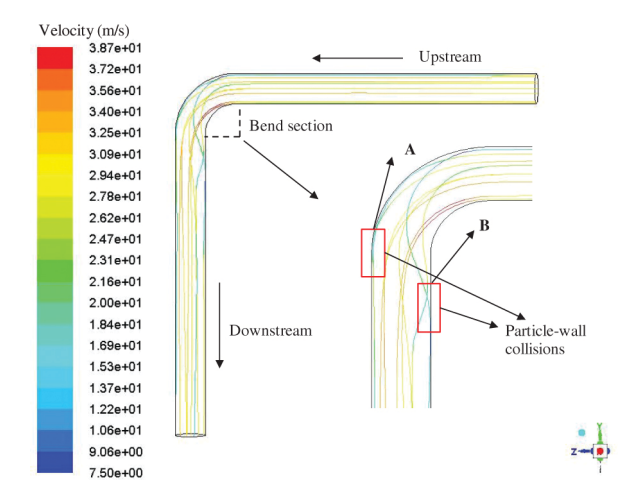


Figure 7: Sample particle velocity trajectories in elbow.

5.7 Effect of secondary flow in elbow

The three-dimensional simulations successfully predicted the presence of strong secondary flow effects at the exit section of the elbow. Figure 8(a-d) illustrates the secondary flow paths by the velocity vectors at the exit section of the elbow for respective oil viscosity conditions. As discussed earlier on, when the fluid flow through the elbow, the velocity field near the intrados is greater than that near the extrados. The circumferential motion of the fluid at the intrados as shown in Figure 8 is due to the strong effect of centrifugal forces as compared to the extrados.

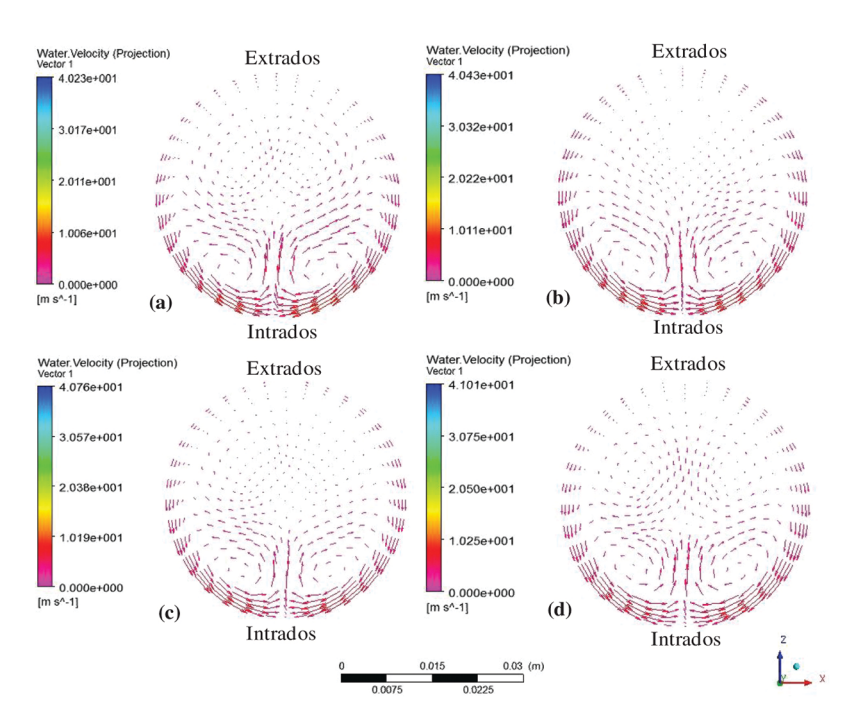


Figure 8: Velocity vectors in the cross-section exit of the bend for different oil viscosity conditions: (a) 0.0572 Pa.s, (b) 0.0911 Pa.s, (c) 0.155 Pa.s, and (d) 0.287 Pa.s.

In addition, the pressure gradient at the extrados is larger than that at the intrados. As an outcome, the flow is directed back from the extrados region to the intrados region near the pipe walls, thus the secondary flow occurs. Therefore, the secondary flow vortices direct a number of solid particles by the surrounding fluid from the intrados region to the extrados region [27]. As a result, severe erosion is observed on the side walls of the downstream straight pipe near the bend exit. According to the velocity vectors, it can clearly be confirmed that the fully developed secondary flows force the particle to impinge on the side wall of a 90-degree bend pipe. Based on this result, the distribution of erosion on the side walls near the bend exit can be justified.

6 Conclusions

A three-dimensional CFD-based numerical simulations of multiphase flow oil-water-sand was conducted to analyse erosion rates in a 90-degree elbow pipe (R/D=1.5), for different engine-oil viscosity conditions. A one-way coupling was adopted for all the simulations, with Eulerian model to simulate the liquid phase (oil-water) and the realizable k- ϵ turbulent model, whereas Lagrangian framework was employed to track the particle's motion. In order to verify the numerical results, the proposed erosion prediction was compared with the experimental data for elbow pipe available in the literature. Based on the simulation results, it was found that the erosion rates decrease with the increase in oil viscosity. The flow characteristic of the liquid phases was found to be a mixed flow. The presence of tiny oil droplets dispersion in the water phase is highly expected with further investigation.

Additionally, the velocity contour plots indicated the presence of high velocity region formed at the intrados of the bend as a result of turbulent effects. However, the pressure was found to be higher at the extrados than in the intrados of the bend due to inertia, and a gradual pressure drop was observed along the flow direction, as a result of friction. The numerical results also showed that, the maximum erosion location was found to be at the exit section of the elbow, which is in reasonable agreement with the experimental observations for 90-degree elbow presented in the literature.

As a general observation, erosion damage mainly occurred in two locations on the elbow. The first location is at the extrados near the bend exit, due to the direct impingement of the particle entrained in the liquid phase. The second location is on the side walls of the downstream straight pipe near the bend exit, as a result of the effects of secondary flow due to centrifugal forces.

Nomenclature

```
3-D Three-dimensional
```

 $A_{\text{face}}\$ Area of cell at the wall subject to erosion (m^2)

 $a_{1,2,3}$ Constants

b(v) Function of relative particle velocity

CFD Computational Fluid Dynamics

 $C_{1,2}$ Constants

 $C(d_P)$ Particle mass flow rate (kg s⁻¹)

C_D Drag coefficient

 C_u Constant

C, *f* , *b* Constant functions

D Pipe diameter (m)

 d_v Diameter of particle (m)

DPM discrete phase model

 e_n Restriction coefficient in normal direction

 e_t Restriction coefficient in tangential direction

F_D Drag force (N)

 F_{φ} Gravity force (N)

 F_p Pressure force (Pa)

 F_{VM} Virtual mass force (N m⁻³)

 $f(\alpha)$ Function of impact angle

 G_k Generation of turbulence kinetic energy due to the mean velocity gradient

g Gravitational acceleration (m s⁻²)

I Unit tensor

k Turbulence kinetic energy (m 2 s $^{-2}$)

 \dot{m}_p Particle mass flow rate (kg s⁻¹)

14

```
P Pressure (Pa)
RANS Reynolds Average Navier-Stokes
R/D Ratio of radius of curvature over the diameter of pipe
SAE oil Society of Automotive Engineers
St Stokes number
S_k, S_{\varepsilon} User defined source terms
t Time (sec)
u_f Velocity of the fluid (m .s<sup>-1</sup>)
u_n Velocity of the particle (m .s<sup>-1</sup>)
u_{pn} Normal velocity component of particle
u_{vt} Tangential velocity component of particle
v Relative particle velocity
x, y Cartesian coordinates (m)
Greek symbols
\varepsilon Dissipation rate of turbulent kinetic energy (m^2 s^{-3})
\alpha_f Volume fraction of fluid
\rho Density (kg m<sup>-3</sup>)
  Stress tensor of fluid (Pa)
μ Dynamic viscosity (Pa s)
\sigma_k, \sigma_{\varepsilon} Turbulent Prandtl numbers
\alpha Particle impact angle (° C)
\phi Maximum erosive angle (° C)
\tau Shear stress (Pa)
Subscripts
f Fluid phase (oil-water)
o Oil
w Water
```

References

p Particle

- [1] Chen], Wang Y, Li X, He R, Han S, Chen Y. Reprint of "Erosion prediction of liquid-particle two-phase flow in pipeline elbows via CFD–DEM coupling method". Powder Technol. 2015;282:25–31.
- [2] Wang K, Li X, Wang Y, He R. Numerical investigation of the erosion behavior in elbows of petroleum pipelines. Powder Technology. 2016;314:490–9
- [3] Liu H, Zhou Z, Liu M. A probability model of predicting the sand erosion profile in elbows for gas flow. Wear. 2015;342–343:377–90.
- [4] Droubi M, Tebowei R, Islam S, Hossain M, Mitchell E Computational Fluid Dynamic Analysis of Sand Erosion in 900 Sharp Bend Geometry. 2016.
- [5] Peng JD, Pak A, Chinello L, Wood T, Low A, editors. Advances in multiphase flow CFD erosion analysis. Offshore Technology Conference. Offshore Technology Conference, 2013.
- [6] Mohyaldin ME, Elkhatib N, Ismail M, editors. Evaluation of different modelling methods used for erosion prediction. Proceedings of the NACE Corrosion Changhai Conference & Expo. 2011.
- [7] Blanchard D, Griffith P, Rabinowicz E. Erosion of a pipe bend by solid particles entrained in water. J Eng Ind(Trans ASME). 1984;106:213–21.
- [8] Solnordal CB, Wong CY, Boulanger J. An experimental and numerical analysis of erosion caused by sand pneumatically conveyed through a standard pipe elbow. Wear. 2015;336–337:43–57.
- [9] Parsi M, Agrawal M, Srinivasan V, Re V, Cf T, Bs M, et al. CFD simulation of sand particle erosion in gas-dominant multiphase flow. J Nat Gas Sci Eng. 2015;27:706–18.
- [10] Mansouri A, Arabnejad H, Shirazi SA, McLaury BS. A combined CFD/experimental methodology for erosion prediction. Wear. 2015;332–333:1090–97.

- [11] Grant G, Tabakoff W. Ohaio: Cincinnati University, Dept. of Aerospace Engineering, An experimental investigation of the erosive characteristics of 2024 aluminum alloy, DOI: Report No. 73-37, 1973. .
- [12] Neilson JH, Gilchrist A. Erosion by a stream of solid particles. Wear. 1968;11:111–22.
- [13] Oka YI, Okamura K, Yoshida T. Practical estimation of erosion damage caused by solid particle impact: part 1: effects of impact parameters on a predictive equation. Wear. 2005;259:95–101.
- [14] DNV. Recommended practice RP O501 Erosive Wear in Piping Systems. DNV Recommended Practice. 2007;4:1–39
- [15] Zhang Y, Reuterfors E, McLaury BS, Shirazi S, Rybicki E. Comparison of computed and measured particle velocities and erosion in water and air flows. Wear. 2007;263:330–38.
- [16] Peng W, Cao X. Numerical simulation of solid particle erosion in pipe bends for liquid—solid flow. Powder Technol. 2016;294:266—79.
- [17] Wang K, Liu Z, Liu G, Yi L, Liu P, Chen M, et al. Vibration sensor approaches for sand detection in oil–water–sand multiphase flow. Powder Technol. 2015;276:183–92.
- [18] Morsi S, Alexander A. An investigation of particle trajectories in two-phase flow systems.] Fluid Mech. 1972;55:193–208.
- [19] Parsi M, Najmi K, Najafifard F, Hassani S, McLaury BS, Shirazi SA. A comprehensive review of solid particle erosion modeling for oil and gas wells and pipelines applications. J Nat Gas Sci Eng. 2014;21:850–73.
- [20] Safaei M, Mahian O, Garoosi F, Hooman K, Karimipour A, Kazi S, et al. Investigation of micro-and nanosized particle erosion in a 90° pipe bend using a two-phase discrete phase model. Sci World J. 2014;2014:1–12
- [21] Mazumder QH. Tutorial: Investigate erosion in a 180 degree u-bend using fluent. Computational Fluid Dynamics Research Center. 2009.
- [22] Nädler M, Mewes D. Flow induced emulsification in the flow of two immiscible liquids in horizontal pipes. Int J Multiphase Flow. 1997;23:55–68.
- [23] Ismail AShamsul I, Ismail I, Zoveidavianpoor M, Mohsin R, Piroozian A, Misnan MS, et al. Review of oil—water through pipes. Flow Meas Instrum. 2015;45:357–74.
- [24] Enayet M, Gibson M, Taylor A, Yianneskis M. Laser-Doppler measurements of laminar and turbulent flow in a pipe bend. Int J of Heat Fluid Flow. 1982;3:213–19.
- [25] Abhari MN, Ghodsian M, Vaghefi M, Panahpur N. Experimental and numerical simulation of flow in a 90 bend. Flow Meas Instrum. 2010;21:292–98.
- [26] Wu H, Liang X, Deng Z. NUMERICAL SIMULATION ON TYPICAL PARTS EROSION OF THE OIL PRESSURE PIPELINE. Thermal Sci. 2013;17:1349–53.
- [27] Feng B, Sun Y, Yang X, Li S, Tu J, Jiang S. Characteristics of helium gas with high temperature and high pressure flowing through a 90-degree elbow. ISRN Power Eng. 2014;2014:1–6
- [28] Tang L, Xiong J, Wan W, Guo Z, Zhou W, Huang S, et al. The effect of fluid viscosity on the erosion wear behavior of Ti(C,N)-based cermets. Ceramics Int. 2015;41:3420–26.
- [29] Kowsari K, James DF, Papini M, Spelt JK. The effects of dilute polymer solution elasticity and viscosity on abrasive slurry jet micromachining of glass. Wear. 2014;309:112–19.
- [30] Parsi M, Vieira RE, Kesana N, McLaury BS, Shirazi SA. Ultrasonic measurements of sand particle erosion in gas dominant multiphase churn flow in vertical pipes. Wear. 2015;328:401–13.